5-14-2008

Theoretical And Experimental Studies Of Collision-Induced Electronic Energy Transfer From v=0-3 Of The E(0g+) Ion-Pair State Of Br2: Collisions With He And Ar

J. M. Hutchison

Robin R. O'Hern

Thomas Alex Stephenson
Swarthmore College, tstephe1@swarthmore.edu

Y. V. Suleimanov

A. A. Buchachenko

Recommended Citation

J. M. Hutchison, Robin R. O'Hern, Thomas Alex Stephenson, Y. V. Suleimanov, and A. A. Buchachenko. (2008). "Theoretical And Experimental Studies Of Collision-Induced Electronic Energy Transfer From v=0-3 Of The E(0g+) Ion-Pair State Of Br2: Collisions With He And Ar". *Journal Of Chemical Physics*. Volume 128, Issue 18. DOI: 10.1063/1.2912057
https://works.swarthmore.edu/fac-chemistry/16

Theoretical and experimental studies of collision-induced electronic energy transfer from v = 0 – 3 of the E (0 g +) ion-pair state of Br 2 : Collisions with He and Ar

J. Matthew Hutchison, Robin R. O'Hern, Thomas A. Stephenson, Yury V. Suleimanov, and Alexei A. Buchachenko

Citation: The Journal of Chemical Physics **128**, 184311 (2008); doi: 10.1063/1.2912057
View online: http://dx.doi.org/10.1063/1.2912057
View Table of Contents: http://scitation.aip.org/content/aip/journal/jcp/128/18?ver=pdfcov
Published by the AIP Publishing

Theoretical and experimental studies of collision-induced electronic energy transfer from $v=0-3$ of the $E(0_g^+)$ ion-pair state of Br_2: Collisions with He and Ar

J. Matthew Hutchison,[1] Robin R. O'Hern,[1] Thomas A. Stephenson,[1,a)]
Yury V. Suleimanov,[2] and Alexei A. Buchachenko[2,b)]
[1]*Department of Chemistry and Biochemistry, Swarthmore College, Swarthmore, Pennsylvania 19081, USA*
[2]*Department of Chemistry, Moscow State University, Moscow 119991, Russia*

(Received 31 January 2008; accepted 27 March 2008; published online 13 May 2008)

Collisions of Br_2, prepared in the $E(0_g^+)$ ion-pair (IP) electronic state, with He or Ar result in electronic energy transfer to the D, D', and β IP states. These events have been examined in experimental and theoretical investigations. Experimentally, analysis of the wavelength resolved emission spectra reveals the distribution of population in the vibrational levels of the final electronic states and the relative efficiencies of He and Ar collisions in promoting a specific electronic energy transfer channel. Theoretically, semiempirical rare gas-Br_2 potential energy surfaces and diabatic couplings are used in quantum scattering calculations of the state-to-state rate constants for electronic energy transfer and distributions of population in the final electronic state vibrational levels. Agreement between theory and experiment is excellent. Comparison of the results with those obtained for similar processes in the IP excited I_2 molecule points to the general importance of Franck–Condon effects in determining vibrational populations, although this effect is more important for He collisions than for Ar collisions. © *2008 American Institute of Physics*.
[DOI: 10.1063/1.2912057]

I. INTRODUCTION

Numerous detailed investigations have revealed the rich electronic energy transfer dynamics that occur when electronically excited diatomic iodine interacts with inert collision partners.[1–18] These studies have focused on the dynamics that accompany the collisions of I_2 following excitation to the $E(0_g^+)$ ion-pair (IP) state and document an important model system for examining nonadiabatic processes in molecules with dense rovibronic energy levels.[17] The E state is one of the six electronic states that constitute the so-called first tier of the IP states; for the first tier, all six states have T_e values that lie within $\approx 1500\ cm^{-1}$ of one another.[19] Collisions with atomic, diatomic, and polyatomic collision partners result in efficient and selective electronic energy transfer to some of the nearby IP states. The initial studies in this field have been the subject of an extensive review article,[17] which highlights the general conclusions of a range of investigations. These studies have focused on gaining an understanding of the branching between the various IP states, and the distribution of population in the vibrational energy manifolds within each electronic state. Briefly, these studies indicate that the electronic energy transfer cross sections increase with increasing vibrational energy within the E state and that the trends in the propensity rules for the distribution of population in vibrational levels also vary with the initial vibrational level within the E state (v_E). This variation can be traced to changes in the distribution of Franck–Condon overlaps and energy gaps between the initial and final vibrational states.

Since the publication of this initial review, additional experimental and theoretical studies have elaborated on these general trends. Akopyan *et al.* have extended the experimental methodology to examine the electronic energy transfer dynamics in the next highest tier of IP states in I_2.[4,7] Their examination of the collision-induced pathways that follow excitation of a range of vibrational levels in the $f(0_g^+)$ state demonstrated that the collision-induced vibrational distributions are consistent with those observed following excitation of the E state. The balancing of the final vibrational distributions between states with small energy gaps with the initial state and those with large Franck–Condon overlap is both delicate and general. The same group also performed a more detailed study of energy transfer from excited vibrational levels of the E state induced by atomic and molecular partners that revealed the dependence of collision dynamics on the nature and strength of the long-range interaction.[3,5,6] In further work, Hutchison *et al.* examined the interaction of I_2 ($v_E=0-2$) with CF_4,[13] and demonstrated that collisions with this polyatomic molecule can result in electronic energy transfer pathways that excite the lowest frequency vibration in CF_4 at low v_E.

In theoretical studies, a special form of intermolecular perturbation theory for quasidegenerate dipole-coupled electronic states was implemented to evaluate inductionlike and electrostatic long-range corrections to interaction potentials and diabatic couplings for colliding particles.[7,14,18] When combined with the quantum scattering approach previously

a)Author to whom correspondence should be addressed. Electronic mail: tstephe1@swarthmore.edu.
b)Electronic mail: alexei@classic.chem.msu.su.

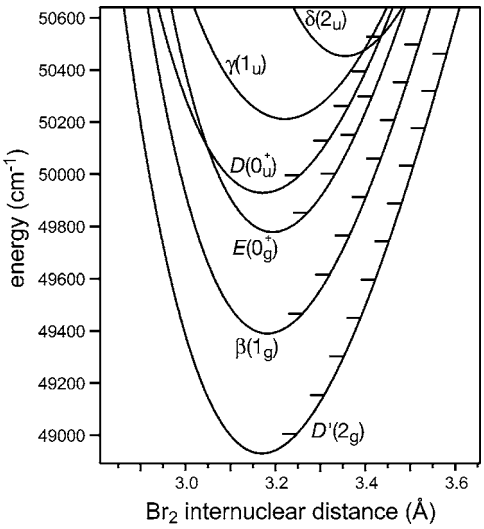

FIG. 1. The first tier of IP states in Br_2. Energy on the vertical axis is relative to T_e of the ground $X(0_g^+)$ state. Vibrational levels are indicated by tick marks at the outer turning points of the four lowest energy electronic states. (See Sec. II for references.)

developed,[16] this improved theory revealed the importance of the long-range interactions in driving collision-induced electronic energy transfer for a range of atomic and molecular collision partners. It also provided very good agreement with the measured rate constants and vibrational product state distributions for collisions with rare gases[18] (Rgs) and with CF_4,[14] allowing a deeper understanding of the role of symmetry, Franck–Condon overlaps, energies of the states involved, and properties of collision partner in the energy transfer dynamics.

With the goal of testing the generality of these experimental and theoretical results, we have now turned our attention to the electronic energy transfer pathways that accompany collisions of Br_2 in the $E(0_g^+)$ state with helium and argon. Br_2 is a particularly favorable candidate to test the conclusions that result from the many studies on I_2 collision dynamics. In Br_2, the IP states are arranged in tiers, just as in I_2, with the lowest tier consisting of six electronic states of the same symmetry as those in I_2.[20] The potential energy curves for these states are displayed in Fig. 1. While the overall electronic character of these states is similar to that of I_2, reduced mass effects dictate that the overall rovibronic state spectrum is less dense. Thus, in Br_2 there are fewer opportunities for accidental resonances (small energy gap pathways) that can influence the electronic energy transfer dynamics. Moreover, there is one significant distinction in the energy ordering of the electronic states: In I_2, the initially prepared E state lies 383 cm^{-1} above the $D(0_u^+)$ state, and $E \rightarrow D$ collision-induced energy transfer is one of the dominant pathways observed, independent of the E state vibrational level initially prepared.[17] In Br_2, however, the D state lies above the E state by 150 cm^{-1}.[20] We expect to observe a strong variation of the cross section for $E \rightarrow D$ electronic energy transfer as we prepare different vibrational levels in the E state. This variation and the resulting D state vibrational population distributions will provide an ideal opportunity to test our emerging understanding of the role of vibronic energy gaps and Franck–Condon overlaps in determining vibrational distributions following collisions with the simplest Rg partners.

TABLE I. Excitation schemes and wavelengths used for the preparation of E state Br_2.

	$B \leftarrow X$		$E \leftarrow B$	
v_E	(v_B, v_X)	λ_1 (nm)	(v_E, v_B)	λ_2 (nm)
0	(13,1)	576.4	(0,13)	312.3
1	(14,1)	572.6	(1,14)	312.0
2	(16,1)	565.5	(2,16)	312.7
3	(17,1)	562.2	(3,17)	312.3

The study of $Br_2(E)$ dynamics is also an important test of the theoretical methodology used in previous investigations. The ability of the theoretical approaches developed for I_2 collisions to properly capture the distinctions in the intermolecular potentials and energy level structure that are relevant to Br_2 collisions will inform future theoretical developments in this area.

II. EXPERIMENT

We use an experimental strategy that is similar to that described in previous publications from our laboratory in Swarthmore.[10–13] Double resonance excitation prepares bromine molecules in a single vibrational level of the E electronic state. A Nd^{3+}:YAG (YAG denotes yttrium aluminum garnet) pumped dye laser system (Continuum Lasers YG580/TDL-50, ~0.15 cm^{-1} bandwidth) produces light resonant with a $B \leftarrow X$ transition (λ_1), and a N_2-pumped dye laser system (Laser Photonics UV24/DL-14P and Inrad Autotracker II system, ~0.25 cm^{-1} bandwidth) produces light resonant with the corresponding $E \leftarrow B$ transition (λ_2). We prepare four different vibrational levels of E state bromine, $v_E = 0-3$. Values for λ_1 and λ_2 as well as vibronic transitions (v', v'') are listed in Table I. We consistently excite hot bands in the $B \leftarrow X$ transitions because significantly increased Franck–Condon factors more than compensate for the lower population of $v_X = 1$ in our room temperature sample.

Excitation of Br_2 vapor occurs in a glass and fused silica cell, equipped with Brewster's angle laser inlet and exit windows. In the experiments reported we use 50 mTorr Br_2 (Aldrich, 99.99%) and a variable pressure of He (GTS, 99.9995%) or Ar (GTS, 99.9995%), typically 500–2000 mTorr. Double resonance excitation of Br_2 results in intense $E \rightarrow B$ fluorescence between 305 and 316 nm, as well as a number of weaker features. We measure Br_2 fluorescence after dispersion through a 0.5 m focal length scanning monochromator (Instruments SA 500M). The exit slit of the monochromator has been replaced with a charge-coupled device (CCD) camera (Princeton Instruments LN/CCD-2500PB) which records a total spectral width of ~24 nm in a single exposure.

We simulate the dispersed fluorescence spectra to extract the distribution of electronic and vibrational states populated through collision-induced electronic energy transfer. Spectroscopic constants were taken from the literature for the elec-

tronic ground state $X(0_g^+)$,[21] excited valence states $A'(2_u)$,[22] $A(1_u)$,[23] and $B(0_u^+)$,[24] and IP states $D'(2_g)$,[22] $\beta(1_g)$,[23] $E(0_g^+)$,[25] and $D(0_u^+)$.[20] Rydberg–Klein–Rees (RKR) potential energy curves were calculated from the spectroscopic constants.[26] These potentials and the Numerov method[27] were used to calculate numerical vibrational wave functions and Franck–Condon factors.

In our previous work on electronic energy transfer in I_2, we were able to prepare single rotational levels of iodine in the E IP state. We achieved this selectivity by exciting a relatively high rotational level ($J=55$) using a peak in the $B \leftarrow X$ vibronic transitions where the rotational fine structure is nearly completely resolved. We are unable to achieve this selectivity with bromine due to the need to excite a relatively low rotational state. The B electronic state of bromine exhibits a strong, rotationally dependent propensity toward predissociation.[28,29] As a result, B state vibronic levels have considerably shorter lifetimes as J increases. Thus, we must excite a transition with a relatively low J value in the $B \leftarrow X$ excitation step to assure that we prepare an adequate population in the E state following absorption of the second photon (λ_2). For all $B \leftarrow X$ transitions listed in Table I, we excite a peak ~ 3 cm^{-1} to the red of the bandhead for the $^{79,81}Br_2$ mixed isotope.

We prepare E state bromine molecules in a small spread of low J rotational states, a result of the spectral complexity near the particular vibronic bandheads and our laser linewidth. In all of our spectral simulations, we have assumed a central rotational quantum number of $J=7$, with any spread in rotational state accounted in the spectral resolution of our monochromator/CCD combination. The quality of our spectral fits does not depend on what J value we assume to be most populated, as long as that value is relatively small ($J<20$).

To test that our reported vibrational distributions result from single collision encounters, we examined each electronic energy transfer pathway as a function of the pressure of the collision partner. In all cases, the intensities of spectral features due to collision-induced electronic energy transfer linearly increase with the pressure of the collision partner. Furthermore, the vibrational distributions are independent of the pressure; both results suggest no significant contribution from multiple collisions. While we did not measure the emission lifetimes of the Br_2 IP states, the corresponding lifetimes for the I_2 IP states are well documented and range from 8 to 26 ns.[30] Assuming similar lifetimes for the Br_2 IP states, our experiments are conducted within the single-collision regime, consistent with our pressure dependent data.

III. THEORY

The theory used to calculate the rate constants and vibrational product state distributions for the nonadiabatic $Br_2(E)$+He, Ar collisions was developed for analogous processes involving iodine molecule, so only a brief outline is given here. The diabatic potential energy surfaces (PESs) and couplings are obtained using a combination of first-order intermolecular diatomics-in-molecule perturbation theory (IDIM PT1) and perturbation theory for the long-range three-body interactions. The IDIM PT1 model is the same as previously described.[17] For its parametrization, we use accurate *ab initio* He, Ar–Br^- interaction potentials computed within the CCSD(T) coupled cluster method with an extended basis set augmented by the bond functions ("Oakland" potentials) from Ref. 31. The He, Ar–Br^+ potentials were calculated in the same manner; we remove the lowest-order induction contributions from both sets of potentials.[17] At long range, the potentials incorporate the inductionlike correction for the strong dipole interaction of the IP states as previously evaluated and applied to the PESs of all states.[7,18]

The interaction PESs and diabatic couplings of the Br_2Rg systems appeared to be very similar to those of I_2Rg.[18] At long range, the PESs are fully determined by the inductionlike interaction between the instantaneous dipole moment of a polarizable Rg atom and the giant transition dipole moment connecting the pairs of IP states that differ only by inversion parity.[32,33] To a good approximation, these moments reflect the resonant charge separation in the IP states and are identical for both halogen molecules. Differences appear only in the short-range IDIM PT1 section, owing mostly to the distinct exchange, dispersion, and high-order induction interactions in the Rg-$Br^{\pm}$ and Rg-$I^{\pm}$ ions. The global van der Waals minimum in all IP states corresponds to the T-shaped configuration of the complex. For Br_2Rg, it is slightly shifted toward shorter distances than in I_2Rg systems. The well depth varies, depending on the particular state, from 50 to 55 cm^{-1} for Br_2He and from 750 to 890 cm^{-1} for Br_2Ar, being approximately 10% larger and 2%–10% smaller than in the iodine analogs, respectively.[18] The diatomic IP states are described using the same RKR potentials as employed for the spectral simulations (see above).

The scattering problem is solved using the electronic and vibrational close coupling rotational infinite-order sudden (EVCC-IOS) approximation for the collisions involving Hund's case (c) molecules.[16] We include all ten components of the six first-tier IP states (two nondegenerate, four doubly degenerate) arising from the double degeneracy of states with nonzero projection of the total molecular angular momentum on the molecule-fixed axis. We incorporate the appropriate number of vibrational states to provide convergence of the smallest vibrationally resolved cross sections within 10%. The initial angular momentum is set to $J=7$ in agreement with the experimental fits.

The EVCC-IOS cross sections are evaluated at ten collision energies from 50 to 1500 cm^{-1}. The standard expression is employed to obtain the rate constants $k_{n'v_{n'} \leftarrow nv_n}$ from the vibrationally resolved cross section (σ) at $T=300$ K:

$$k_{n'v_{n'} \leftarrow nv_n}(T) = \left(\frac{8}{\pi \mu k_B T}\right)^{1/2} \int (k_B T)^{-1} E \sigma_{n'v_{n'} \leftarrow nv_n}(E) \times \exp[-E/k_B T] dE, \quad (1)$$

where n and n' refer to the initial and final electronic states, $v_{n'}$ and v_n to the corresponding vibrational levels, and k_B is the Boltzmann constant. Vibrational product state distributions are calculated as

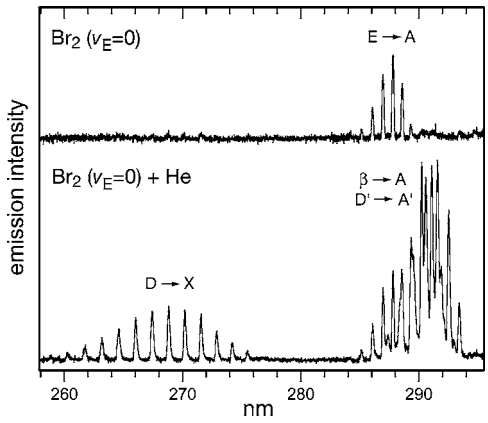

FIG. 2. Dispersed fluorescence spectra of Br_2 between 258 and 295 nm obtained after excitation to $v_E=0$. The top spectrum is from a 50 mTorr sample of pure bromine vapor and shows emission only from the state we prepare, while the lower spectrum is from a sample of 50 mTorr Br_2 mixed with 1500 mTorr He and includes emission from other electronic states populated through collision with He.

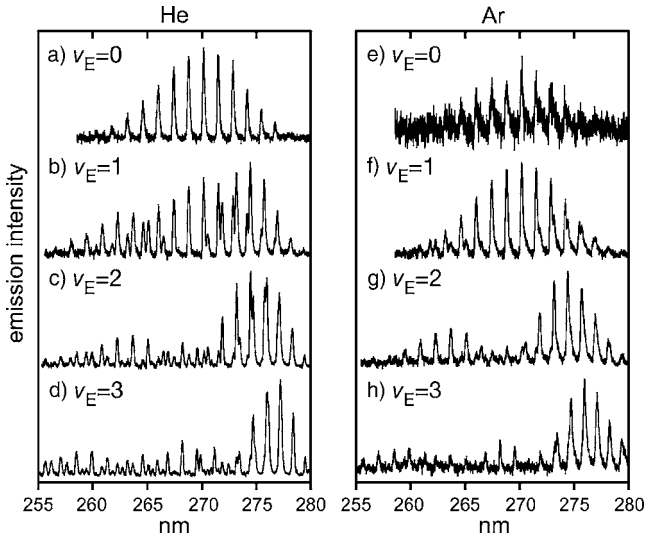

FIG. 3. $D \rightarrow X$ emission between 255 and 280 nm of Br_2 excited to $v=0-3$ in the E state. The pressure for He (left-hand side) or Ar (right-hand side) is 1500 mTorr in all samples. As the initial vibrational level is increased (top to bottom in the figure), emission maxima move toward longer wavelengths, indicative of transitions from correspondingly higher vibrational levels of the D state.

$$P_{n'\leftarrow nv_n}(v_{n'}) = \frac{k_{n'v_{n'}\leftarrow nv_n}(T)}{\Sigma_{v_{n'}} k_{n'v_{n'}\leftarrow nv_n}(T)}. \quad (2)$$

IV. EXPERIMENTAL AND THEORETICAL RESULTS

The top half of Fig. 2 shows the relatively weak $E(0_g^+) \rightarrow A(1_g)$ emission of Br_2 after excitation to $v_E=0$. (The dominant $E(0_g^+) \rightarrow B(0_u^+)$ emission occurs at slightly longer wavelengths.) In behavior similar to I_2, collisions with either He or Ar induce transitions in $Br_2(E)$ to the neighboring D', β, and D IP states. Upon introduction of He or Ar gas to our sample cell, fluorescence due to collision-induced energy transfer dominates the emission spectrum between 250 and 300 nm. The bottom half of Fig. 2 shows the fluorescence from a cell filled with 50 mTorr Br_2 and 1500 mTorr He, in which Br_2 molecules have been excited to the state $v_E=0$. Prominent spectral features in all fluorescence spectra after collision with He or Ar include $D(0_u^+) \rightarrow X(0_g^+)$ emission between 255 and 280 nm and the overlapping $\beta(1_u) \rightarrow A(1_g)$ and $D'(2_g) \rightarrow A'(2_u)$ emissions between 284 and 295 nm.

Collisions of Br_2 in low vibrational levels of the E state with the He or Ar atoms induce energy transfer into a range of vibrational levels in the D', β, and D electronic IP states. To extract the distribution of vibrational levels populated through collision-induced energy transfer in a given electronic state, we perform spectral simulations of the fluorescence spectra, where the populations of the vibrational levels in the given electronic state are variable parameters.

A. $E \rightarrow D$ transfer

Emission spectra from the D state are shown in Fig. 3. We find $D \rightarrow X$ emission under all conditions involving the collision of Br_2 ($v_E=0-3$) and He [Figs. 3(a)–3(d)] or Ar atoms [Figs. 3(e)–3(h)]. Each spectrum contains a series of peaks from a collection of vibrational levels of the D state whose population depend on the initially prepared v_E level and identity of the collision partner. We find that collisions lead to significant population in only a narrow envelope of one to three vibrational levels in the D state and that this envelope moves to larger vibrational levels of the D state as we change our initially prepared level from $v_E=0$ to $v_E=3$.

The intensity of the emission spectra in this region appears to be quite different for He and Ar collisions. While we have normalized all the spectra in Fig. 3, emission intensity differences are apparent in the relative signal-to-noise ratios [for example, between Figs. 3(a) and 3(e)]. The improved signal-to-noise ratio observed when He is the collision partner suggests that Br_2+He collisions are more likely to populate the D state than Br_2+Ar collisions. (As discussed below, the strength of this conclusion is complicated by uncertainties associated with normalizing the D state spectra to account for the number of molecules initially excited to the E state.) This observation is similar to that observed in $I_2(E)$ +He, Ar collision-induced electronic energy transfer, where $E \rightarrow D$ state transfer is preferred in He collisions. The other striking difference—seen most clearly in Figs. 3(b)–3(f)—is that He and Ar collisions generate different spectral features. As discussed below, these differences are a direct reflection of D state vibrational populations that vary with the collision partner.

A qualitative analysis of the $D \rightarrow X$ spectra is based on considering the characteristics of the X and D state potential energy curves, which have significantly different minimum bond lengths (2.28 and 3.17 Å, respectively).[20,21] Thus, the low vibrational levels of the D state have significant Franck–Condon overlap only with the outer turning point of the X state potential at high vibrational levels ($v_X=35-60$). As a result, emission spectra from selected vibrational levels of the D state tend to resemble the shape of the D state wave function. For example, emission spectra after excitation to $v_E=0$, Figs. 3(a) and 3(e), contain only a single progression

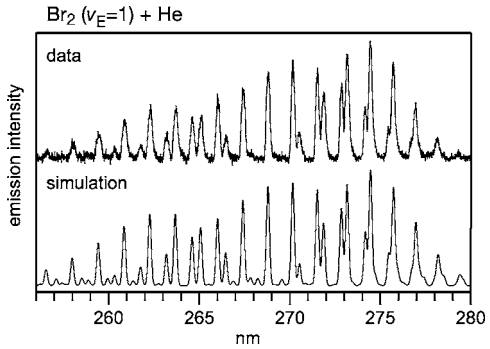

FIG. 4. Experimental (top) and spectroscopic simulation (bottom) of the $D \rightarrow X$ emission of 50 mTorr $Br_2(v_E=1)$+1500 mTorr He. The simulation uses a basis of emission spectra from $v_D=0-4$ and a bandwidth of 0.12 cm^{-1}, which accurately accounts for the peak widths of the top spectrum. The spectrum contains roughly equal contributions from $v_D=0$ and 1.

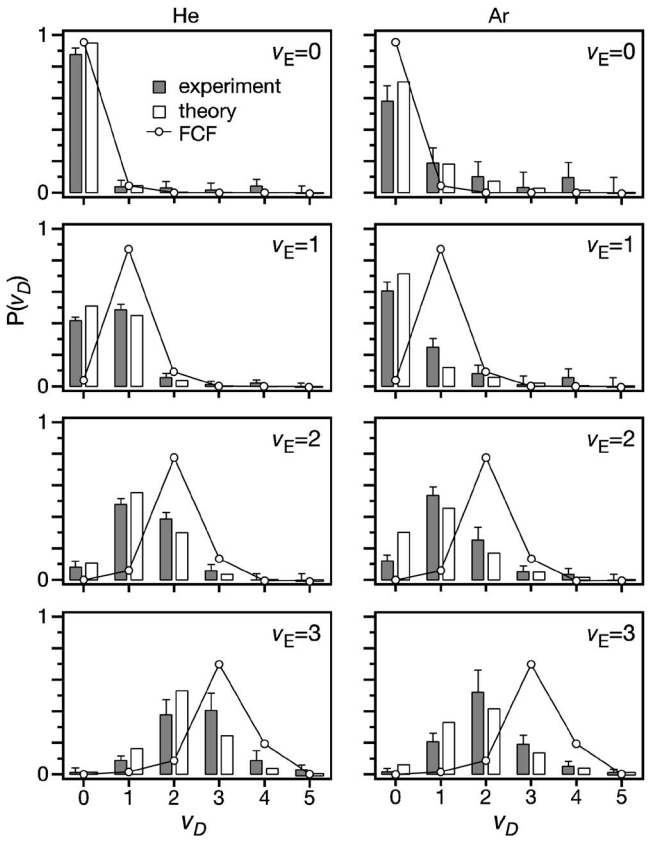

FIG. 5. Experimental (gray) and theoretical (white) D state vibrational distributions following $E \rightarrow D$ collision-induced electronic energy transfer in $Br_2(v_E=0-3)$ with He (left-hand side) and Ar (right-hand side). Franck–Condon factors between the initially prepared v_E level and v_D are shown as open circles. For $v_E=0-2$, $P(v_D=5)$ are set to zero in fitting the experimental spectra.

of peaks with maxima near 270 nm, features indicative that the majority of the total emission is from $v_D=0$. As the initially prepared state, v_E, is increased, the maximum intensity shifts to longer wavelengths, indicative of emission from higher vibrational levels of the D state, whose wave functions have maximum amplitude at their turning points.

As an example of our spectral fits, Fig. 4 shows both the experimental (top half) and simulated (bottom half) $D \rightarrow X$ emission following $Br_2(v_E=1)$+He collision-induced electronic energy transfer. Just as in the spectrum in Fig. 3(a), there is a progression of peaks with a maximum near 270 nm that originates from $v_D=0$. However, the spectrum in Fig. 4 has an additional contribution from a bimodal series of peaks with maxima near 262.2 and 274.5 nm, indicative of emission from $v_D=1$. Our simulation accurately reproduces all of the spectral features above and indicates a roughly equal contribution from population of the two lowest vibrational levels of the D state. Our spectral fits allow for the emission from $v_D=0-4$ and the small, additional peaks in the bottom half of Fig. 4 are mostly due to a contribution from $v_D=2$. While these peaks are not observed above the noise level in the measured spectrum, their presence in the fit gives us an estimate of the inherent uncertainty of our simulation and vibrational level population distributions.

Figure 5 shows the D state vibrational level populations following $E \rightarrow D$ transfer extracted from spectral simulations and through our EVCC-IOS calculations. Following the presentation in Fig. 3, distributions resulting from collision with He are shown on the left, while those following collision with Ar are on the right. Results from increasing the initially prepared v_E are presented from top to bottom. From these distributions, it clear that E state bromine displays markedly different behavior from the comparable results from $I_2(E)$ +He, Ar.[10,12] Whereas He and Ar collisions produced similar vibrational state distributions in the IP pair states of iodine, our present results show markedly different dynamics between collisions of the Rgs with bromine.

Superimposed on the vibration state distributions in Fig. 5 are Franck–Condon factors between the initially prepared state v_E and final state v_D. Because the r_e values of the E and D potentials differ by only 0.02 Å, the maximum Franck–Condon factors occur between levels with the same vibrational quantum number. There is, however, increased Franck–Condon overlap to additional vibrational levels as v_E increases. We find that He collisions are more likely to result in transitions to v_D levels with large Franck–Condon factors, whereas Ar collisions are more likely to populate v_D levels with one less vibrational quantum than the initial v_E level. Given that the E and D state potential curves are displaced in energy roughly by one unit of vibrational energy (Fig. 1), we thus observe that Ar collisions are more likely to induce a transition that minimizes the energy gap between v_E and v_D.

These trends are best observed by comparing the v_D distributions from the initial states $v_E=0$ and $v_E=1$. At $v_E=0$ both He and Ar induce transitions primarily to $v_D=0$, a state 142 cm^{-1} higher in energy; however, this change is much more dominant upon collision with He. There is a near degeneracy at $v_E=1$, where $v_D=0$ lies just 7 cm^{-1} lower in energy. Here, Ar still primarily induces transitions to $v_D=0$; however, the emission intensity is significantly larger, suggesting that energy resonance is an important factor in Br_2 +Ar collision dynamics. He collisions, on the other hand, induce transitions to both $v_D=0$ and $v_D=1$, indicating that both minimizing the energy gap and maximizing Franck–Condon overlap drive the energy transfer. This trend continues at $v_E=2$ and 3; however, the product state distributions become broader and more similar between He and Ar as the initial state goes to higher vibrational levels. Energy gaps

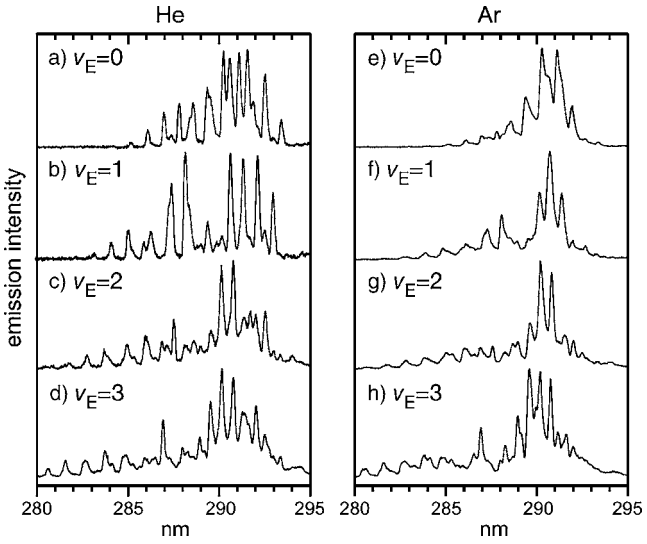

FIG. 6. Emission between 255 and 280 nm for Br_2 excited to $v=0-3$ in the E state, which contains overlapping $E\rightarrow A$, $\beta\rightarrow A$, and $D'\rightarrow A'$ transitions. The pressure of He (left-hand side) or Ar (right-hand side) is 1500 mTorr in all samples.

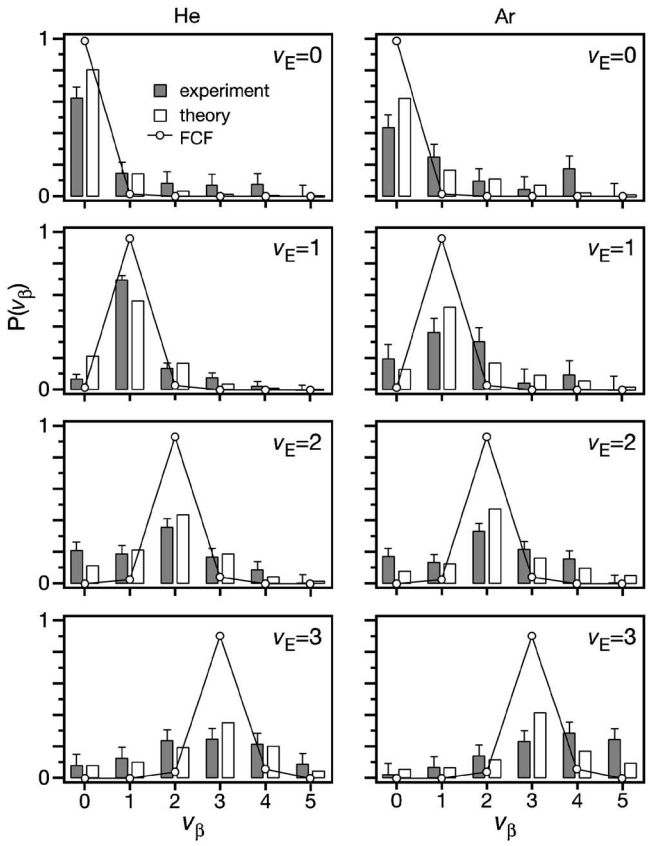

FIG. 7. Experimental (gray) and theoretical (white) β state vibrational distributions following $E\rightarrow\beta$ collision-induced electronic energy transfer in $Br_2(v_E=0-3)$ with He (left-hand side) and Ar (right-hand side). Franck–Condon factors between the initially prepared v_E level and v_β are shown as open circles. For $v_E=0-2$, $P(v_\beta=5)$ are set to zero in fitting the experimental spectra.

between v_E and the D state vibrational levels with one less quanta get larger as v_E increases; however, even at $v_E=3$, we still see a clear preference for He collisions to populate $v_D=3$ over Ar collisions.

We see excellent agreement between experiment and theory for both He and Ar collisions at all energy levels studied. Discrepancies are more prominent at larger ν_E levels; however, this may be due to the experimental error of the spectral fits being significantly greater at higher energies. As the number of D state vibrational levels populated increases, it becomes increasingly difficult to unambiguously assign certain spectral features to exact ν_D levels. However, even where experiment and theory disagree on the population of a specific vibrational level, there is clear agreement that Ar collisions populate lower vibrational levels in the D state than He collisions.

B. $E\rightarrow D'$ and $E\rightarrow\beta$ transfer

Fluorescence spectra between 280 and 295 nm contain emission from both the β and D' electronic states. Figure 6 shows that collisions with He (left-hand side) or Ar (right-hand side) result in distinctly different emission spectra. Spectral simulations of the $\beta\rightarrow A$ and $D'\rightarrow A'$ emission reveal that He and Ar collisions result in different branching ratios for transfer to the β and D' states. We find that He collisions result in spectra with a roughly equal contribution from the β and D' state emission, while Ar collisions result in spectra containing a majority of emission from the β state.

We produce better quality spectral fits for spectra resulting from He collisions, where we can accurately reproduce all peaks from $\beta\rightarrow A$ and $D'\rightarrow A'$ emission. For Ar collision spectra, there are several peaks near 290 nm in all spectra with an unresolved baseline that we are unable to reproduce when only considering emission from the lower energy IP states. It is possible that, in these cases, there is a small and broad contribution to the total emission from the higher energy δ and γ IP states; however, there is no known spectroscopic information for such transitions. Despite this limitation, we are able to reproduce the intensities of the large peaks that are unambiguously assigned to β state emission. Consequently, we only consider the well known emission from the β and D' states in our spectral simulations.

Figures 7 and 8 show vibrational state distributions in the β and D' states, respectively, after preparation of $\nu_E=0-3$. Just as in our $D\rightarrow X$ fits, we only include emission from $\nu_n=0-4$ ($n=\beta$ or D') for spectra originating from $\nu_E=0-2$ and include $\nu_n=0-5$ for spectra originating from $\nu_E=3$. We find that the quality of the fits does not improve when including emission from additional vibrational levels. Our theoretical studies do consider transfer to a larger number of vibrational levels in all cases; however, we have only shown the vibrational state distributions to $\nu_n=0-5$ for the benefit of comparison to experiment. The very small contribution of D' state emission in the Ar collision spectra, combined with the unresolved baseline features, results in large errors in our vibrational state distributions in the D' state for these experiments.

The experimental and theoretical vibrational state distributions in Figs. 7 and 8 agree very well. In transfer to the β state (Fig. 7), we see a preference for transfer to states with large Franck–Condon factors; however, the distributions are broader than those observed in the D state, described above.

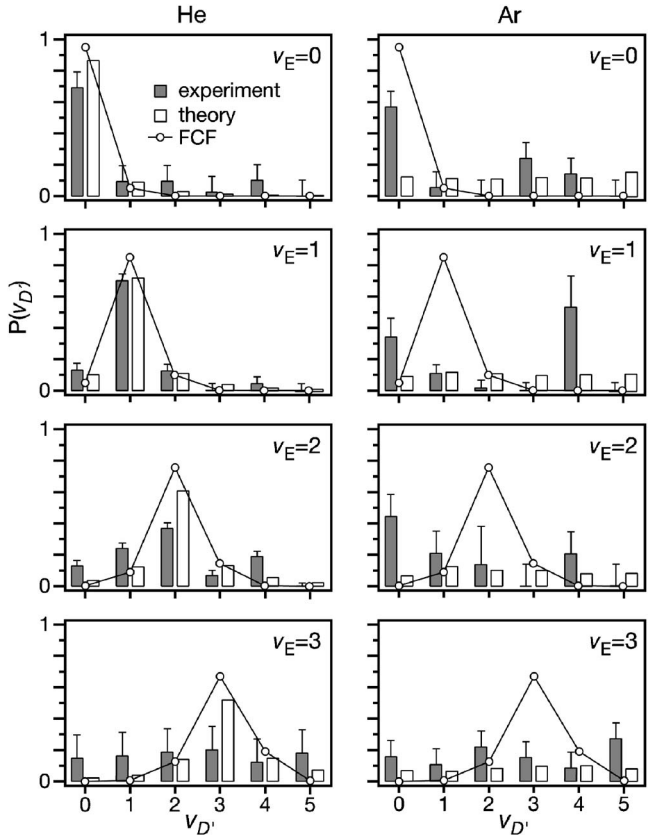

FIG. 8. Experimental (gray) and theoretical (white) D' state vibrational distributions following $E \rightarrow D'$ collision-induced electronic energy transfer in $Br_2(v_E=0-3)$ with He (left-hand side) and Ar (right-hand side). Franck–Condon factors between the initially prepared v_E level and v_D are shown as open circles. For $v_E=0-2$, $P(v_D=5)$ are set to zero in fitting the experimental spectra. For Ar, theory assigns a significant fraction of the total population to $v_{D'}>5$ levels (not shown).

Similar to the D state distributions, the distributions broaden, and Franck–Condon effects are lessened as the initial v_E level increases. Also similar to $E \rightarrow D$ transfer, there is a greater Franck–Condon agreement with He collisions, rather than those with Ar. Collisions with Ar are more likely (relative to He collisions) to transfer population to states with $v_\beta > v_E$—energy transfer paths with smaller energy gaps than those with large Franck–Condon overlap—again, similar to the behavior seen in transfer to the D state.

The D' state distributions in Fig. 8 show the same trend in He collisions. As described above, the distributions following Ar collisions have considerable error and do not show any discernible trends. Experimental and theoretical distributions agree only in that both show very broad distributions, especially at larger v_E levels. Indeed, theoretical computations consider transfer to a very wide range of vibrational levels and find very broad and even distributions, although they do see a slight preference for transfer to states with a minimum energy gap. Conversely, He collisions do show a pronounced preference for transfer to states with large Franck–Condon overlap; however, this preference weakens as v_E increases. Indeed, once the initial state is as high as $v_E=3$, the experimental populations show the same broad distribution observed with Ar collisions.

The strong preference for transfer to states with large Franck–Condon factors in both the β and D' states when He is the collision partner indicates that there are minimal energy gap effects in the energy transfer process. The ΔT_e values between the E and β or D' states are 387 and 845 cm^{-1}, respectively. For both electronic states, all of the final state levels with non-negligible Franck–Condon overlap involve substantial energy gaps with the initially prepared E state vibrational levels. As in the case of collisions with $I_2(E)$ +He and Ar,[10,12] collisions of $Br_2(E)$+He direct population into levels with large energy gaps and large vibrational overlaps rather than near-resonant levels with small overlaps. The striking difference between the halogens is that Ar and He collisions produce much the same result when colliding with I_2, but different distributions when interacting with Br_2.

TABLE II. Theoretical total rate constants (10^{-17} m^3 s^{-1} $molecule^{-1}$) for collisionally induced electronic energy transfer from the given initial vibrational levels to the final electronic states D', β, and D.

Final state	Initial E state level			
	$v_E=0$	$v_E=1$	$v_E=2$	$v_E=3$
		Br_2+Ar		
D'	3.1	3.2	3.2	3.3
β	3.0	3.1	3.2	3.2
D	4.7	12	20.5	29
		Br_2+Ar		
D'	2.2	2.3	2.4	2.1
β	15	14	14	12
D	1.0	5.1	7.8	12

C. Rate constants for electronic energy transfer

The calculated rate constants for the observed collision-induced transitions are listed in Table II. The theory shows that the nonadiabatic transitions between the IP states of Br_2 are very efficient: The rate constant values for the dominating channels are as high as 3×10^{-16} m^3 s^{-1} $molecule^{-1}$. For collisions with He, the $E \rightarrow D$ energy transfer dominates, whereas the $E \rightarrow \beta$ and $E \rightarrow D'$ transitions have equal but smaller probability. The rate constant for the former transition rapidly increases with v_E, while the latter two seem to be almost independent of initial excitation. Collisions with Ar exhibit the same dependence on v_E, but in contrast to He, the most efficient transition at $v_E<3$ occurs to the β state, in qualitative agreement with experimental observations (see below).

Unlike our previous experimental investigations of the electronic energy transfer dynamics of $I_2(E)$,[10–13] we are unable to extract either absolute or relative rate constants from our experimental data on $Br_2(E)$ collisions. In the case of I_2, the radiative rate constants for all six of the first-tier IP states have been measured along with the electronic transition moments for each of the transitions used in our analysis.[30] These data made it possible to quantify the competition between radiative relaxation of the E state and collision-induced electronic energy transfer. The data also provided a mechanism for calculating the absolute, final state specific energy transfer rate constants from our experimental intensities.[10–13] The

TABLE III. Experimental and theoretical collision gas dependent rate constant ratios, k_{Ar}/k_{He}, for transfer from the given v_E level to the different electronic states.

Initial state	Final electronic state		
	D	β	D'
$v_E=0$	1.0 ± 0.5[a]	7.7 ± 1.4	1.65 ± 0.4
	0.21[b]	5.0	0.71
$v_E=1$	0.30 ± 0.05	4.8 ± 0.5	1.04 ± 0.16
	0.42	4.5	0.72
$v_E=2$	0.28 ± 0.05	2.0 ± 0.3	0.66 ± 0.13
	0.38	4.4	0.75
$v_E=3$	0.31 ± 0.10	1.7 ± 0.5	0.8 ± 0.2
	0.41	3.8	0.64

[a]Experimental.
[b]Calculated.

corresponding measurements of the radiative rate constants for the Br_2 IP states are not available. As a result, we cannot make a precise comparison with the theoretically determined energy transfer rate constants. By assuming that the variation in the Br_2 radiative rate constants is no more significant than that in I_2, however, our experimental intensities are qualitatively in accord with the trends in the theoretical energy transfer rate constants described above.

We are able, however, to compare the dependence of specific electronic energy transfer channel rate constants on the Rg collision partner. In Table III, we list the rate constant ratios k_{Ar}/k_{He} for the final electronic states considered. The agreement with the theoretical calculations is quite good, confirming that He collisions are more effective (relative to Ar collisions), in general, of populating the D state, while Ar collisions are more effective (relative to He collisions) at populating the β state. In some cases, the experimental error bars are higher than desired. Our analysis requires normalization of the D, β, and D' state emission intensity to the intensity of the $E\rightarrow A$ emission (Fig. 2). In the case of Ar collisions, however, strong emission from the β state [Figs. 6(e)–6(h)] made precise measurement of the E state emission intensity difficult.

The theoretical calculations indicate the existence of energy transfer pathways to the higher energy δ and γ IP states. According to our results, the corresponding rate constants do not exceed 10^{-18} m^3 s^{-1} $molecule^{-1}$ for He and 10^{-17} m^3 s^{-1} $molecule^{-1}$ for Ar, but rapidly grow with v_E. As previously noted, unassigned features in our experimental spectra may result from δ and/or γ state emission when Ar is the collision partner, but these features are absent when He is the collision partner. This tentative result is consistent with the relative magnitudes of the theoretically determined energy transfer rate constants.

V. DISCUSSION

Both experimental and theoretical results reveal that Franck–Condon and energy gap trends have somewhat different weights for $Br_2(E)$ collisions with He and Ar. Comparison with similar processes in the $I_2(E)$ molecule previously studied by using the same methods allows further analysis of their relative importance.[10,12,17,18] It is worthwhile to stress once again that the diabatic PESs and couplings for these systems are very similar; so differences in the dynamics should be expected to arise from the peculiarities of the IP state energy level structure.

As shown in Figs. 5, 7, and 8, for each of the final IP states (D,D',β), the distributions of Franck–Condon factors with the E state possess sharp maxima. These maxima adjoin or coincide with the quasiresonant vibrational level of the final electronic state (D state) or are energetically distant (D' and β states). In the I_2 molecule the Franck–Condon distributions are significantly broader, a difference that is not reflected in the vibrational distributions for the $E\rightarrow\beta$ and $E\rightarrow D'$ transitions for I_2 and Br_2, since Franck–Condon factors dominate the final state population distribution regardless of the actual size of the vibrational overlaps.[10,12] However, the $E\rightarrow D$ transitions create sharply different vibrational distributions in the two molecules. In I_2, low initial v_E levels and the final D state levels v_D with the minimum energy gap have very small Franck–Condon factors (e.g., $\langle v_E=0|v_D=4\rangle^2=4\times10^{-4}$) that suppress the quasiresonant energy transfer.[10,12] In Br_2, quasiresonant levels v_D lie very close to the maximum of the Franck–Condon distribution ($v_E=1-3$) or even coincide with it ($v_E=0$). The synergy of the energy gap law and the Franck–Condon principle results not only in the predominance of the quasiresonant energy transfer but also in a significant increase in the rate constant values. The same synergy was observed in the I_2 molecule for $E\rightarrow D$ transitions at higher v_E levels[3] and for $f\rightarrow F$ transitions in the second tier of IP states.[7] For example, the $f,v_f=14\rightarrow F$ transition in I_2 resembles very much the $E,v_E=0\rightarrow D$ transition in Br_2. The final vibrational level $v_F=14$ of the F state that corresponds to the smallest energy gap simultaneously has the maximum Franck–Condon overlap with initial state and is by far the most populated.[7] With an initial excitation to $v_f=17$, the nearest level $v_F=17$ is one level removed from the level with maximum vibrational overlap. The experimental results are similar to the transitions from the $v_E=1-3$ levels in the Br_2 molecule.

The nonadiabatic transitions from the E state in bromine are much more efficient than those in iodine, by one to two orders of magnitude for He and by at least an order of magnitude for Ar, according to comparable theoretical calculations.[18] The rate constants for $E\rightarrow D$ transitions listed in Table II are close to those measured (and calculated) for the abovementioned $f\rightarrow F$ transitions in I_2 and can be explained by considering the synergy between the energy gap law and the Franck–Condon principle.[7] The large rate constants for the $E\rightarrow\beta$ and $E\rightarrow D'$ transitions cannot be rationalized in this way, however. Our previous theoretical calculations[16] indicate that, for I_2 collisions, the β and D' states are indirectly populated via the intermediate D state. For Br_2+Ar collisions, we carried out similar EVCC-IOS calculations in which different subspaces of the vibronic basis set expansion are included.[16] These calculations also reveal the critical role of the D state as an intermediate in the population of the β and D' states in Br_2. Thus, the increase in the $E\rightarrow D$ transition probability from iodine to bromine naturally leads to a simultaneous increase in the $E\rightarrow\beta$ and $E\rightarrow D'$ probability. For this reason, the differences in the

Franck–Condon distributions and energy gaps in the two molecules alter the vibrational product state distributions and rate constants, but not the branching between the electronic states. An analysis of the present theoretical data and the results of measurements and calculations for the iodine molecule[10,12,18] points out that the electronic branching ratios for the two molecules are indeed very similar.

An unresolved issue in our analysis is the possible role of rotational energy transfer in smoothing, to some extent, the sharp propensities in Franck–Condon factors and vibronic energy gaps. Experimentally, the rotational energy conditions for I_2 and Br_2 are rather different, with single excitation of $J=55$ in the case of I_2 and excitation of multiple rotational states centered at low J in Br_2. The rotor constants for the molecules differ by more than a factor of 2, and this difference combined with the inconsistency in initial state preparation could contribute to the changes in vibrational distributions that we observe. Unfortunately this aspect is impossible to theoretically clarify by using the present approach, which invokes the infinite-order sudden approximation to rotational energy transfer.[34,35]

In any case, our theoretical approaches starting from semiempirical construction of the analytical PESs and diabatic couplings and ending with quantum scattering calculations provide very good agreement with the experimental results on the $Br_2(E)$+Rg collisions. This success is an elaboration of that previously obtained for $I_2(E)$+Rg (Ref. 18) and $I_2(f)$+Rg (Ref. 7) collisions. These results justify the application of similar methods to a wide range of nonadiabatic collision-induced processes occurring in the excited states of heavy diatomic molecules.

VI. SUMMARY

The electronic energy transfer dynamics that accompany collisions of $Br_2(E)$ with He and Ar have been experimentally and theoretically examined, with excellent agreement between the investigations. Collisions with He and Ar induce electronic energy transfer to the D, D', and β IP states, although the relative rate constants substantially vary. He collisions favor population of the D state, while Ar collisions direct population predominately to the β state, results that are both consistent with previous studies of $I_2(E)$ collisions.[10,12] The vibrational distributions within each electronic state vary with the identity of the collision partner, with He collisions populating vibrational levels with significant Franck–Condon overlap with the initial E state vibrational level. On the other hand, collisions with Ar favor population in vibrational levels that are closer in energy to the initially prepared level. Collision-induced population of the D state occurs with a rate constant in Br_2 than is significantly larger than the corresponding process in I_2,[18] a result of the existence of energy transfer pathways that simultaneously maximize the Franck–Condon overlap and minimize the vibronic energy gap. The agreement between theory and experiment is a hopeful sign that the methodology developed to date is adequate to quantitatively apply to a wide range of nonadiabatic processes.

ACKNOWLEDGMENTS

We thank Dr. Timur V. Tscherbul for his interest and valuable assistance. Our theoretical work (Moscow) is supported by the Russian Basic Research Fund (Project Nos. 05-03-32371 and 08-03-00352) and Russian Science Support Fund (to A.A.B.). Our experimental work (Swarthmore) is supported by grants from the Research Corporation, the Camille and Henry Dreyfus Foundation Scholar/Fellow program, and the Swarthmore College Faculty Research Fund.

Acknowledgment is made to the Donors of the American Chemical Society Petroleum Research Fund for partial support of this research.

[1] M. E. Akopyan, N. K. Bibinov, D. B. Kokh, A. M. Pravilov, O. L. Sharova, and M. B. Stepanov, Chem. Phys. **263**, 459 (2001).
[2] M. E. Akopyan, N. K. Bibinov, D. B. Kokh, A. M. Pravilov, M. B. Stepanov, and O. S. Vasyutinskii, Chem. Phys. **242**, 263 (1999).
[3] M. E. Akopyan, A. A. Buchachenko, S. S. Lukashov, S. A. Poretsky, A. M. Pravilov, Y. V. Suleimanov, A. S. Torgashkova, and T. V. Tscherbul, Chem. Phys. Lett. **436**, 1 (2007).
[4] M. E. Akopyan, I. Y. Chinkova, T. V. Fedorova, S. A. Poretsky, and A. M. Pravilov, Chem. Phys. **302**, 61 (2004).
[5] M. E. Akopyan, S. S. Lukashov, E. I. Khadikova, E. A. Nikandrova, S. A. Poretsky, A. M. Pravilov, and A. S. Torgashkova, Chem. Phys. **342**, 173 (2007).
[6] M. E. Akopyan, S. S. Lukashov, Y. D. Maslennikova, S. A. Poretsky, A. M. Pravilov, and A. S. Torgashkova, Chem. Phys. Lett. (in press).
[7] M. E. Akopyan, I. Y. Novikova, S. A. Poretsky, A. M. Pravilov, A. G. Smolin, T. V. Tscherbul, and A. A. Buchachenko, J. Chem. Phys. **122**, 204318 (2005).
[8] M. E. Akopyan, A. M. Pravilov, M. B. Stepanov, and A. A. Zakharova, Chem. Phys. **287**, 399 (2003).
[9] N. K. Bibinov, O. L. Malinina, A. M. Pravilov, M. B. Stepanov, and A. A. Zakharova, Chem. Phys. **277**, 179 (2002).
[10] P. P. Chandra and T. A. Stephenson, J. Chem. Phys. **121**, 2985 (2004).
[11] C. J. Fecko, M. A. Freedman, and T. A. Stephenson, J. Chem. Phys. **115**, 4132 (2001).
[12] C. J. Fecko, M. A. Freedman, and T. A. Stephenson, J. Chem. Phys. **116**, 1361 (2002).
[13] J. M. Hutchison, B. R. Carlisle, and T. A. Stephenson, J. Chem. Phys. **125**, 194313 (2006).
[14] Y. V. Suleimanov and A. A. Buchachenko, J. Phys. Chem. A **111**, 8959 (2007).
[15] T. V. Tscherbul and A. A. Buchachenko, Chem. Phys. Lett. **370**, 563 (2003).
[16] T. V. Tscherbul and A. A. Buchachenko, J. Phys. B **37**, 1605 (2004).
[17] T. V. Tscherbul, A. A. Buchachenko, M. E. Akopyan, S. A. Poretsky, A. M. Pravilov, and T. A. Stephenson, Phys. Chem. Chem. Phys. **6**, 3201 (2004).
[18] T. V. Tscherbul, Y. V. Suleimanov, and A. A. Buchachenko, Russ. J. Phys. Chem. **80**, 1957 (2006).
[19] J. C. D. Brand and A. R. Hoy, Appl. Spectrosc. Rev. **23**, 285 (1987).
[20] T. Ishiwata, T. Hara, K. Obi, and I. Tanaka, J. Phys. Chem. **95**, 2763 (1991).
[21] C. Focsa, H. Li, and P. F. Bernath, J. Mol. Spectrosc. **200**, 104 (2000).
[22] T. A. Van Marter, Y. Lu, M. C. Heaven, E. Hwang, P. J. Dagdigian, and J. Tellinghuisen, J. Mol. Spectrosc. **177**, 311 (1996).
[23] E. Hwang, P. J. Dagdigian, and J. Tellinghuisen, J. Mol. Spectrosc. **181**, 297 (1997).
[24] R. E. Franklin, C. D. Holmberg, J. R. Reynolds, and G. P. Perram, J. Mol. Spectrosc. **184**, 273 (1997).
[25] J. C. D. Brand, U. D. Deshpande, A. R. Hoy, and S. M. Jaywant, J. Mol. Spectrosc. **100**, 143 (1983).
[26] R. J. Le Roy, *University of Waterloo Chemical Physics Research Report No*. CP-657R, 2004.
[27] I. N. Levine, *Quantum Chemistry*, 4th ed. (Allyn and Bacon, Boston, 1991).
[28] M. A. A. Clyne and M. C. Heaven, J. Chem. Soc., Faraday Trans. 2 **74**, 1992 (1978).
[29] M. A. A. Clyne, M. C. Heaven, and E. Martinez, J. Chem. Soc., Faraday

Trans. 2 **76**, 405 (1980).
[30] K. Lawley, P. Jewsbury, T. Ridley, P. Langridge-Smith, and R. Donovan, Mol. Phys. **75**, 811 (1992).
[31] A. A. Buchachenko, J. Klos, M. M. Szczesniak, G. Chalasinski, B. R. Gray, T. G. Wright, E. L. Wood, L. A. Viehland, and E. Qing, J. Chem. Phys. **125**, 064305 (2006).
[32] K. Lawley, Chem. Phys. **127**, 363 (1988).
[33] A. M. Sjodin, T. Ridley, K. P. Lawley, and R. J. Donovan, J. Chem. Phys. **120**, 2740 (2004).
[34] G. A. Parker and R. T. Pack, J. Chem. Phys. **68**, 1585 (1978).
[35] D. J. Kouri, in *Atom-Molecule Collision Theory*, edited by R. B. Bernstein (Plenum, New York, 1979), p. 301.